Supplementary Information

Asymmetric electron distribution induced intrinsically strong anisotropy of thermal transport in bulk CrOCl

Qikun Tian,[1] Qi Yang,[1] An Huang,[1] Bo Peng,[1] Jinbo Zhang,[1] Xiong Zheng,[1] Jian Zhou,[1] Zhenzhen Qin,[2] and Guangzhao Qin[1*]

[1] *State Key Laboratory of Advanced Design and Manufacturing Technology for Vehicle, College of Mechanical and Vehicle Engineering, Hunan University, Changsha 410082, P. R. China*

[2] *Key Laboratory of Materials Physics, Ministry of Education, School of Physics, Zhengzhou University, Zhengzhou 450001, P. R. China*

[*] gzqin@hnu.edu.cn

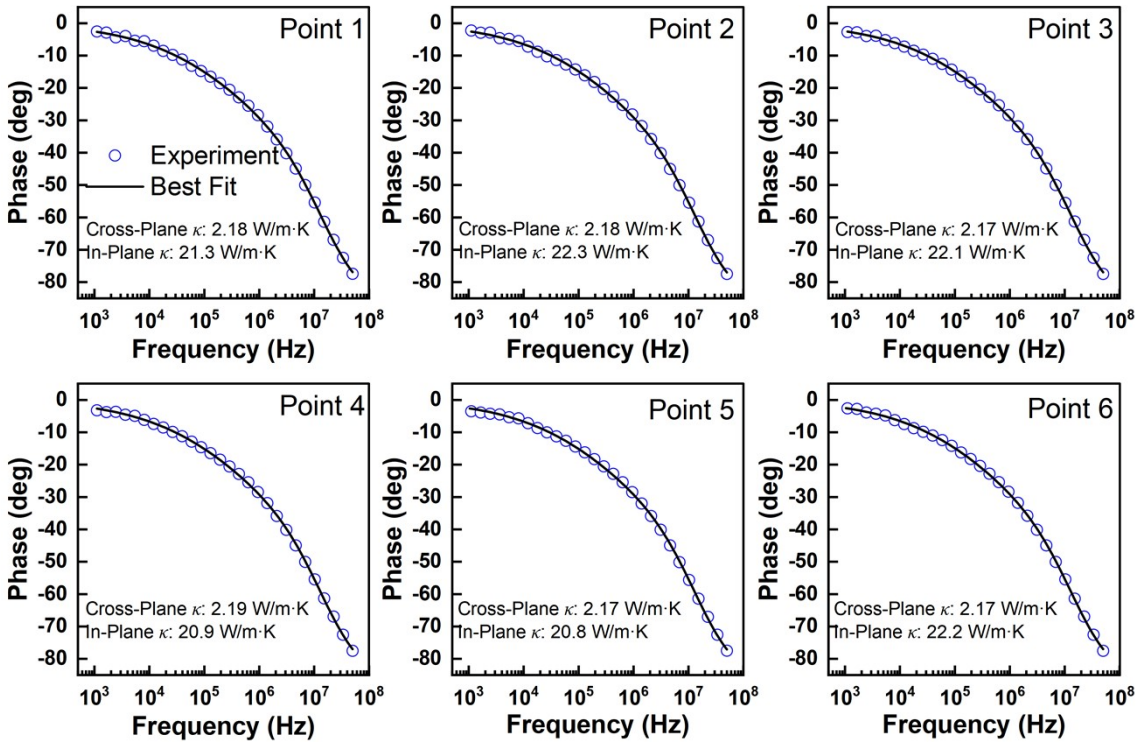

Figure S1 Frequency domain thermoreflectance (FDTR) phase data obtained from six random points on the CrOCl sample. The blue circles represent data points and the solid black line represents data model.

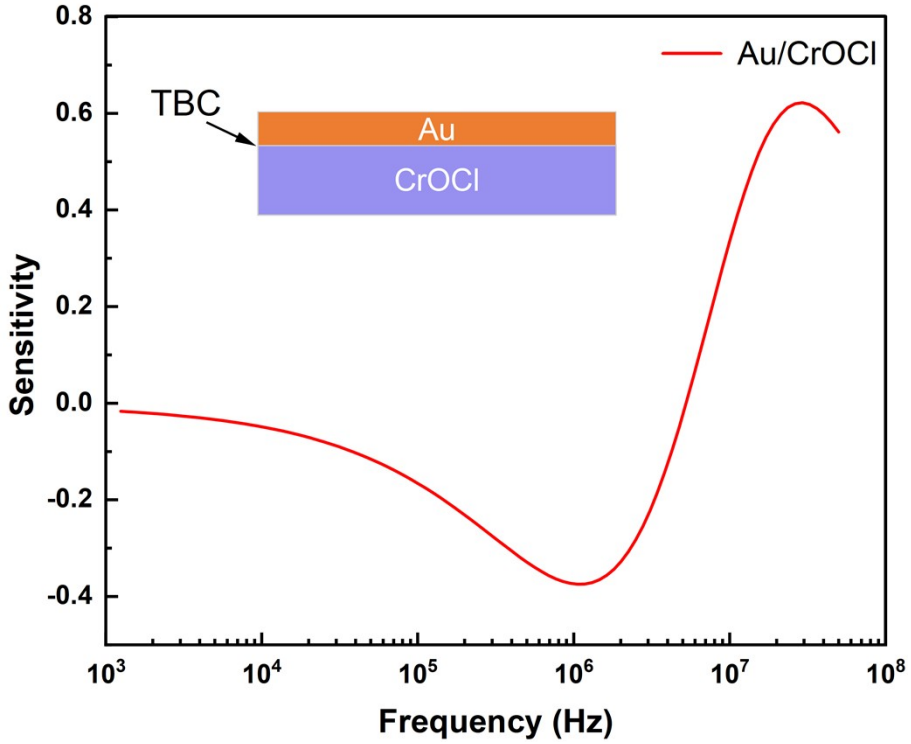

Figure S2 Sensitivity analysis of thermal phase about thermal boundary conductance (TBC) at 300 K. The inset is the schematic of TBC for Au/CrOCl.

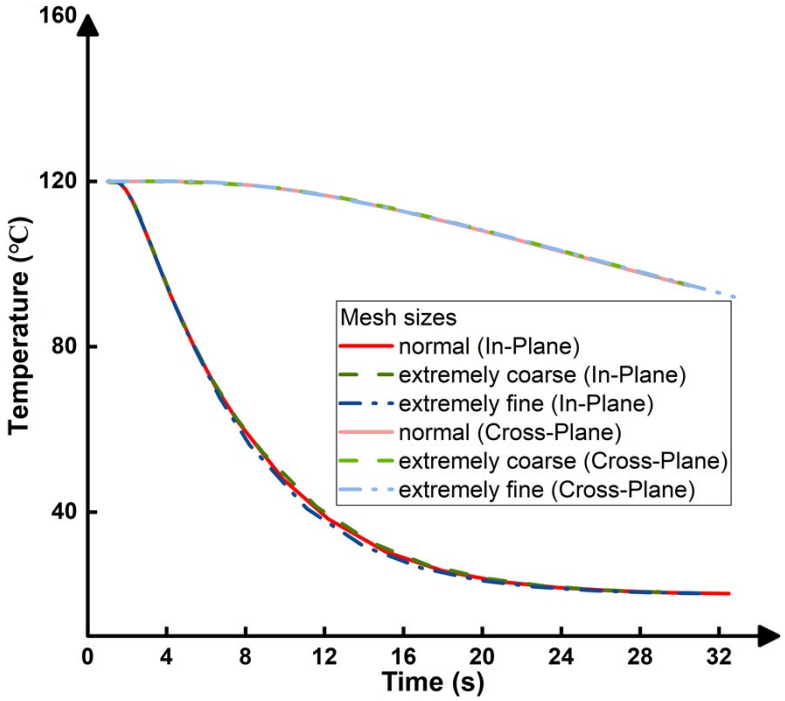

Figure S3 Temperature evolution with respect to time along the in-plane and cross-plane directions, respectively, including three predefined mesh sizes: normal, extremely coarse, and extremely fine.

The mesh independence study was performed using tetrahedral elements with three predefined mesh sizes: extremely coarse, normal, and extremely fine. The results demonstrated that the solution achieved convergence with the normal mesh size. Consequently, the normal mesh size was adopted for finite element simulations, ensuring both computational efficiency and result accuracy.

Table S1 Calculated structural and electronic properties of bulk CrOCl: lattice parameters (Å), electronic band gap E_g (eV) obtained using GGA and GGA+U methods, and employed energy cutoff (Encut, eV). Available experimental values are shown for comparison.

Crstal	State	Space group	a	b	c	E_g	Approach	U	Encut	References
Bulk CrOCl	AFM	*Pmmn*	3.198	3.885	7.698	1.01	GGA	0	600	This work
			3.233	3.918	7.774	2.14	GGA+U	3	600	This work
			3.256	3.940	7.820	2.63	GGA+U	5	600	This work
			3.193	3.882	7.635	1.07	GGA	0	450	Ref. [1]
			3.264	3.947	7.711	2.71	GGA+U	7	450	Ref. [1]
			3.168	3.852	7.755	2.8	Experiment	/	/	Ref. [2,3]

The pure GGA method shows limitations in accurately describing the electronic and structural properties of bulk CrOCl, particularly underestimating the band gap compared to experimental measurements. Through careful comparison with available experimental data and reference calculations, we identified that while the value of U-J =3 eV yields lattice parameters in agreement with experiment, it produces a band gap of 2.14 eV that still significantly underestimates the experimental value of 2.8 eV. The value of U-J=5 eV provides better agreement for both structural parameters and electronic band gap. The obtained lattice constants are consistent with the experimental measurement while producing a band gap of 2.63 eV that closely approaches the experimental value of 2.8 eV, demonstrating that the ground state of bulk CrOCl crystals is well-reproduced. Therefore, in the study on the phonon properties of bulk CrOCl, the GGA+U approach (with U-J=5 eV) was adopted for all the calculations.

Table S2 Measured thermal conductivities κ_a, κ_b, and κ_c ($Wm^{-1}K^{-1}$) along the *a*-direction, *b*-direction, and *c*-direction and anisotropic ratio κ_a/κ_b, κ_a/κ_c for typical bulk materials using experimental methods. FDTR: frequency domain thermoreflectance, TDTR: time-domain thermoreflectance, TM: Thermoreflectance microscopy, LFA: laser-flash analysis.

Bulk materials	κ_a	κ_b	κ_c	κ_a/κ_b	κ_a/κ_c	Methods	References
CrOCl	21.6	-	2.18	-	10	FDTR	This work
Graphite	1983	-	6.1	-	325	TDTR	Ref. [4]
BP	83	28	6.5	3	13	TDTR	Ref. [5]
h-BN	420	-	4.8	-	87.5	TDTR	Ref. [6]
MoS_2	82	-	4.75	-	17	TDTR	Ref. [7]
$MoSe_2$	35	-	2.6	-	13	TDTR	Ref. [7]
$MoTe_2$	19	-	2.5	-	7.6	TDTR	Ref. [8]
WS_2	120	-	2.8	-	43	TDTR	Ref. [7]
WSe_2	42	-	2.2	-	19	TDTR	Ref. [7]
WTe_2	13.5	-	1.34	-	10	TDTR	Ref. [9]
Bi_2Se_3	3.5	-	0.85	-	4	TM	Ref. [10]
Bi_2Te_3	1.8	-	0.9	-	2	LFA	Ref. [11]
4H-SiC	345	-	415	-	0.83	TDTR	Ref. [12]
6H-SiC	320	-	390	-	0.82	TDTR	Ref. [12]
AlN	289	-	283	-	1.02	Three-sensor 2ω	Ref. [13]
GaN	206	-	201	-	1.02	Three-sensor 2ω	Ref. [13]
ZnO	40	-	47	-	0.85	LFA	Ref. [14]
β-Ga_2O_3	9.5	22.5	13.3	0.4	0.7	TDTR	Ref. [15]

Table S3 Calculated Young's modulus E_a, E_b, E_c (GPa) along the *a*-direction, *b*-direction, and *c*-direction and elastic constants C_{ij} (GPa) for typical bulk materials. [d] Calculated results of E_a, E_c from equations [16,17] for

Bulk materials	E_a	E_b	E_c	C_{11}	C_{12}	C_{13}	C_{33}	C_{44}	C_{66}	C_{22}	C_{23}	C_{55}	References
CrOCl	187.5	-	25.9	162.2	28.8	12.4	27.2	11.5	48.7	228.9	10.6	11.4	This work
Graphite	1149[d]	-	36.8[d]	1211.3	275.5	0.6	36.8	4.2	468	-	-	-	Ref. [18]
BP	149.7	45.3	47.0	179.3	38.9	6.3	45.5	55.6	12.7	52.5	0.07	3.9	Ref. [19]
h-BN	812[d]	-	29[d]	853	187	0	29	8	-	-	-	-	Ref. [20]
MoS_2	208.3	-	47.5	221.9	53	9.2	48.2	14.9	84.5	-	-	-	This work
$MoSe_2$	164.7	-	43.5	174.4	38.2	9.8	44.4	14.5	68.1	-	-	-	This work
$MoTe_2$	114.8	-	37	122.1	27	9.0	38.1	18.1	47.6	-	-	-	This work
WS_2	225.8	-	49.8	237.6	50.5	9.4	50.4	14.8	93.6	-	-	-	This work
WSe_2	185.8	-	46.4	193.4	34.5	9.9	47.3	16.2	79.5	-	-	-	This work
WTe_2	129.3	-	40	134	20.7	9.3	41.1	20.3	56.7	-	-	-	This work
Bi_2Se_3	59.5	-	21.8	79.1	21.5	17.1	27.6	18.1	28.8	-	-	-	This work
Bi_2Te_3	49.4	-	23.3	71.2	17.6	19.5	31.9	25.1	26.8	-	-	-	This work
4H-SiC	462.9	-	525.1	488.2	104.1	51.1	533.9	158.3	192.1	-	-	-	This work
6H-SiC	460.1	-	525.5	485.8	105	51.3	534.4	160.7	190.4	-	-	-	This work
AlN	318.7	-	316.4	375	127.8	97.9	354.6	112.1	123.6	-	-	-	Ref. [21]
GaN	288.6	-	346.6	345.9	128.3	93.5	383.5	92.9	108.8	-	-	-	Ref. [21]
ZnO	122.5	-	138.9	189.8	102.2	93.7	199.1	45.2	43.8	-	-	-	Ref. [22]
β-Ga_2O_3	136.7	250.1	242.3	209.8	108.1	113.5	307.8	45.9	89.2	312.2	65.8	65.2	This work

hexagonal crystals, where $E_a = 2\left(\frac{C_{33}}{C} + \frac{1}{C_{11}-C_{12}}\right)^{-1}$, $E_c = \frac{C}{C_{11}+C_{12}}$, $C = C_{33}(C_{11}+C_{12}) - 2C_{13}^2$.

As confirmed by the Born stability criteria [23], the bulk CrOCl satisfies all required conditions:

(i) $C_{11} > 0$,

(ii) $C_{11}C_{22} > C_{12}^2$,

(iii) $C_{11}C_{22}C_{33} + 2C_{12}C_{13}C_{23} - C_{11}C_{23}^2 - C_{22}C_{13}^2 - C_{33}C_{12}^2 > 0$,

(iv) $C_{44} > 0$, $C_{55} > 0$, $C_{66} > 0$.

These results clearly demonstrate the mechanical stability of bulk CrOCl.

REFERENCES

[1] N. Miao, B. Xu, L. Zhu, J. Zhou, and Z. Sun, 2D Intrinsic Ferromagnets from van der Waals Antiferromagnets, J. Am. Chem. Soc. **140**, 2417 (2018).

[2] L. Coïc, M. Spiesser, P. Palvadeau, and J. Rouxel, Chromium (III) oxyhalides : Magnetic and optical properties. Lithium intercalation, Materials Research Bulletin **16**, 229 (1981).

[3] C. H. Maule, J. N. Tothill, P. Strange, and J. A. Wilson, An optical investigation into the $3D^1$ and $3d^2$ transition-metal halides and oxyhalides, compounds near to delocalisation, J. Phys. C: Solid State Phys. **21**, 2153 (1988).

[4] A. J. Schmidt, X. Chen, and G. Chen, Pulse accumulation, radial heat conduction, and anisotropic thermal conductivity in pump-probe transient thermoreflectance, Review of Scientific Instruments **79**, 114902 (2008).

[5] B. Sun, X. Gu, Q. Zeng, X. Huang, Y. Yan, Z. Liu, R. Yang, and Y. K. Koh, Temperature Dependence of Anisotropic Thermal-Conductivity Tensor of Bulk Black Phosphorus, Advanced Materials **29**, 3 (2017).

[6] P. Jiang, X. Qian, R. Yang, and L. Lindsay, Anisotropic thermal transport in bulk hexagonal boron nitride, Phys. Rev. Materials **2**, 6 (2018).

[7] P. Jiang, X. Qian, X. Gu, and R. Yang, Probing Anisotropic Thermal Conductivity of Transition Metal Dichalcogenides MX_2 (M = Mo, W and X = S, Se) using Time-Domain Thermoreflectance, Advanced Materials **29**, 1701068 (2017).

[8] H. Li, T. Pandey, Y. Jiang, X. Gu, L. Lindsay, and Y. K. Koh, Origins of heat transport anisotropy in MoTe2 and other bulk van der Waals materials, Materials Today Physics **37**, 101196 (2023).

[9] X. Qian, P. Jiang, P. Yu, X. Gu, Z. Liu, and R. Yang, Anisotropic thermal transport in van der Waals layered alloys WSe2(1- *x*)Te2 *x*, Applied Physics Letters **112**, 241901 (2018).

[10] D. Fournier, M. Marangolo, M. Eddrief, N. N. Kolesnikov, and C. Fretigny, Straightforward measurement of anisotropic thermal properties of a Bi_2Se_3 single crystal, J. Phys.: Condens. Matter **30**, 11 (2018).

[11] K. Ahn, J. K. Won, Y. K. Kang, C. Hwang, I. Chung, and M.-G. Kim, Thermoelectric properties of nano-bulk bismuth telluride prepared with spark plasma sintered nano-plates, Current Applied Physics **19**, 97 (2019).

[12] Q. Zheng, C. Li, A. Rai, J. H. Leach, D. A. Broido, and D. G. Cahill, Thermal conductivity of GaN, $\$^{71}\mathrm{GaN}\$$, and SiC from 150 K to 850 K, Phys. Rev. Mater. **3**, 1 (2019).

[13] G. Yang and B.-Y. Cao, Three-sensor 2ω method with multi-directional layout: A general methodology for measuring thermal conductivity of solid materials, International Journal of Heat and Mass Transfer **219**, 124878 (2024).

[14] X. Liang and C. Wang, Electron and phonon transport anisotropy of ZnO at and above room temperature, Applied Physics Letters **116**, 4 (2020).

[15] P. Jiang, X. Qian, X. Li, and R. Yang, Three-dimensional anisotropic thermal conductivity tensor of single crystalline β-Ga2O3, Applied Physics Letters **113**, 23 (2018).

[16] D. Tromans, Elastic anisotropy of hcp metal crystals and polycrystals, (2011).

[17] S. S. Bhat, U. V. Waghmare, and U. Ramamurty, First-Principles Study of Structure, Vibrational, and Elastic Properties of Stoichiometric and Calcium-Deficient Hydroxyapatite, Crystal Growth & Design **14**, 6 (2014).

[18] K. H. Michel and B. Verberck, Theory of the elastic constants of graphite and graphene, Physica Status Solidi (b) **245**, 2177 (2008).

[19] G. Qin, Q.-B. Yan, Z. Qin, S.-Y. Yue, H.-J. Cui, Q.-R. Zheng, and G. Su, Hinge-like structure induced unusual properties of black phosphorus and new strategies to improve the thermoelectric performance, Sci Rep **4**, 6946 (2014).

[20] X.-Y. Ren, C.-X. Zhao, C.-Y. Niu, J.-Q. Wang, Y. Jia, and J.-H. Cho, First-principles study of the crystal structures and physical properties of H18-BN and Rh6-BN, Physics Letters A **380**, 3891 (2016).

[21] A. Chen, D. Wei, J. Xu, A. Li, H. Wang, Z. Qin, and G. Qin, Alloying Reversed Anisotropy of Thermal Transport in Bulk Al0.5Ga0.5N, J. Phys. Chem. Lett. **14**, 9746 (2023).

[22] S. S. Bhat, U. V. Waghmare, and U. Ramamurty, Effect of oxygen vacancies on the elastic properties of zinc oxide: A first-principles investigation, Computational Materials Science **99**, 133 (2015).

[23] F. Mouhat and F.-X. Coudert, Necessary and sufficient elastic stability conditions in various crystal systems, Phys. Rev. B **90**, 224104 (2014).